



Assimilating water column and satellite data

X. Yao and R. Schlitzer

# Assimilating water column and satellite data for marine export production estimation

X. Yao and R. Schlitzer

Alfred Wegener Institute Helmholtz Centre for Polar and Marine Research, Columbusstrasse, Bremerhaven, Germany

Received: 30 January 2013 – Accepted: 28 February 2013 – Published: 11 March 2013

Correspondence to: X. Yao (yao.xiaoping@awi.de)

Published by Copernicus Publications on behalf of the European Geosciences Union.

Title Page

Abstract

Introduction

Conclusions

References

Tables

Figures



Back

Close

Full Screen / Esc

Printer-friendly Version

Interactive Discussion



## Abstract

Recent advances in satellite retrieval methodology now allow estimation of particular organic carbon (POC) concentration in ocean surface waters directly from satellite-based optical data. Because of the good coverage these data reveal small-scale spatial and temporal concentration gradients and document the evolution of surface water POC as well as the underlying driving biogeochemical processes throughout the seasons. Water column nutrient data also reveal biogeochemical activity. However, because of the scarcity of data the deduction of temporal changes of particle production and export are not possible in most parts of the ocean. Here we present first results from a new study combining both data streams thereby exploiting the high spatio-temporal resolution of surface POC concentrations from satellite optical sensors with water column nutrient data having sparser coverage but providing information throughout the entire water column. We use a medium-resolution global model with steady-state 3-D circulation that has been optimized by fitting to a large number of hydrographic parameters and tracers, including CFCs and natural radiocarbon. Production and export of POC is allowed to vary monthly, and the magnitudes of the monthly export fluxes are determined by fitting the model to satellite POC data as well as water column nutrient data using the adjoint method. Two cases have been investigated: (1) the production rate of POC is set to be proportional to export production EP and the seasonal changes are assumed sinusoidal (meridionally varying amplitude and phase) and (2) the POC production rate is linked to primary production rates (literature). Both cases were run with the same initial state and model settings, and show total cost function decreases of 12 and 95 %, respectively. The POC misfit term alone decreased by 75 and 99 %. The integrated annual global POC exports of the two cases are  $9.9 \text{ GtCyr}^{-1}$  and  $12.3 \text{ GtCyr}^{-1}$ , respectively. Overall, the remaining POC and phosphate misfits of both solutions are considered too large and the difference fields still exhibit significant systematic geographical patterns. This indicates that the present model runs are too

GMDD

6, 2045–2085, 2013

## Assimilating water column and satellite data

X. Yao and R. Schlitzer

Title Page

Abstract

Introduction

Conclusions

References

Tables

Figures



Back

Close

Full Screen / Esc

Printer-friendly Version

Interactive Discussion



simplistic and do not fully explain the data. Further, more refined model setups are needed.

## 1 Introduction

The ocean is one of the major carbon reservoirs on Earth, containing around 40 000 GtC, about 50 times more than in the atmosphere (Sarmiento and Sundquist, 1992). The ocean is believed to be the ultimate sink for about 90 % of human fossil fuel emissions (Archer et al., 1998). In the surface ocean phytoplankton fixes dissolved carbon to form particulate biomass by photosynthesis (primary production PP). A fraction of the particulate material is sinking into the deep ocean due to gravity thereby sustaining a downward flux of particulate nutrients and carbon (export flux). This process, which depletes the ocean surface of nutrients and dissolved inorganic carbon (DIC) relative to the deep-water, is referred to as the biological pump (Volk and Hoffert, 1985). Drawdown of surface carbon concentrations by the biological pump leads to an increased flux of CO<sub>2</sub>. From the atmosphere, and the overall oceanic CO<sub>2</sub> uptake thus depends on the strength of the biological pump. Quantification of export flux and the strength of the biological pump therefore is an important objective.

Over the past decades extensive work has been carried out to quantify the downward carbon export in the ocean. One observational approach is the use of sediment traps (Honjo et al., 2008; Gardner, 2000; Kahler and Bauerfeind, 2001). This is a direct way of measuring downward export fluxes by capturing and preserving the sinking material. However, the disadvantages are sparse coverage in space and time. Moreover, the catchment efficiency of sediment traps especially in the shallow waters are debated (Gust et al., 1994) casting doubt on absolute flux values derived from shallow traps. Additionally, there is another alternative instrument of measuring carbon export directly, it is carried on ARGO floats, called “Carbo-ARGO” floats (Bishop and Wood, 2009). Besides these direct measurement approaches, radioisotope <sup>234</sup>Th is also widely utilized

## Assimilating water column and satellite data

X. Yao and R. Schlitzer

Title Page

Abstract

Introduction

Conclusions

References

Tables

Figures

⏪

⏩

◀

▶

Back

Close

Full Screen / Esc

Printer-friendly Version

Interactive Discussion



to quantify particle export out of the surface layer (Buesseler et al., 2009; Rutgers v. d. Loeff et al., 2011).

In addition to observational approaches, modeling is a powerful way of quantifying carbon export. Different model approaches are used to estimate carbon export, such as ecosystem models (Aumont et al., 2003; Oschlies and Kähler, 2004) or coupled physical-biogeochemical models (Palmer and Totterdell, 2001). Performance of these forward models in terms of how well measured distributions are simulated highly depends on clever choices of model parameters, such as primary production and functions that relate export flux with PP. The inverse model of Schlitzer (2000, 2002) avoids these parameter choices and treats the geographically varying annual export fluxes as independent parameters determined by the model by exploiting historical water column data. However, this approach only yields the annual average fluxes and does not reveal seasonal changes.

Recent advances in remote sensing now allow direct quantification of surface carbon parameters such as the concentrations of particulate organic carbon (POC) (Stramski et al., 2008) and particulate inorganic carbon (PIC) (Balch et al., 2005; Gordon et al., 2001). The satellite-derived fields are provided globally at high spatial and temporal resolution, and coverage is excellent, especially when compared to ship-based water column data. Both of these quantities are sensitive to biological production and export, therefore analysis of this new data product likely helps revealing flux variations on small space and time scales. The disadvantage is that satellite sensors only monitor the ocean surface. A combination of satellite and water column data can build up a full 4-D view of the global ocean.

The present study, uses the data-driven inverse model developed by Schlitzer (1993, 2000, 2002, 2007) to link water column and satellite data for estimating carbon export and its seasonality. Based on the older model version, we set up a new model combining water column phosphate and satellite POC data in the adjoint model, in order to get better carbon export estimations on a monthly basis. The model is calculated

## GMDD

6, 2045–2085, 2013

### Assimilating water column and satellite data

X. Yao and R. Schlitzer

Title Page

Abstract

Introduction

Conclusions

References

Tables

Figures



Back

Close

Full Screen / Esc

Printer-friendly Version

Interactive Discussion



in phosphor units, and using a constant Redfield ratio (Redfield et al., 1963; Anderson and Sarmiento, 1994) relating between phosphor and carbon.

This paper is structured as follows: In Sect. 2 we introduce the data we used in our study, in Sect. 3 we describe the details of the method of the adjoint model approach, Sect. 4 describe the two experiments we did, Sect. 5 shows the analysis of the results of two experiments, and Sect. 6 contains Summary and Conclusion.

## 2 Data

There are two kinds of data used in this study, dissolved inorganic nutrients ( $C_{Dd}$ ) and particulate ( $C_{Pd}$ ) data. The dissolved inorganic nutrients refer to ship-based observational water column data, which cover the whole global ocean and have vertical coverage. The particulate data are derived from satellites monitoring the ocean from space. These data contain better spatial and temporal coverage than water column data, but only for the ocean surface. Combining these two data types is the novel feature of the present study.

### 2.1 Water column data

The World Ocean Atlas 2009 nutrients (WOA09) (Garcia et al., 2010) is based on a compilation of all presently available cruise observation data under international data collection projects. It is a set of objectively analyzed climatological fields. It has a  $1^\circ$  grid horizontal resolution at standard depth levels for annual, seasonal, and monthly compositing periods for the world ocean. It is a long historical accumulation of water column data in oceanography, which contain important scientific information. They reflect the ocean physical processes as well as biogeochemical information of nutrients. The nutrients water column data show the carbon concentrations and dynamics qualitatively well. In Fig. 1, which takes the ocean surface June and December phosphate at 10 m as examples, we can see that phosphate concentrations in the subtropics are very low

## Assimilating water column and satellite data

X. Yao and R. Schlitzer

Title Page

Abstract

Introduction

Conclusions

References

Tables

Figures



Back

Close

Full Screen / Esc

Printer-friendly Version

Interactive Discussion



---

## Assimilating water column and satellite data

X. Yao and R. Schlitzer

---

Title Page

Abstract

Introduction

Conclusions

References

Tables

Figures

⏪

⏩

◀

▶

Back

Close

Full Screen / Esc

Printer-friendly Version

Interactive Discussion



because of a high activity of plankton using up nutrients in these areas. In the Northern Pacific mid-latitudes and polar region, we can clearly see the seasonal variety of phosphate. In June, the phosphate concentrations are low, whereas in December they are relatively high. In the Northern Hemisphere summer time there is plenty of light and the proper temperature for phytoplankton photosynthesis. In these regions plankton are more active in June, therefore they consume more nutrients in summer than in winter time. Overall water column data have a good global coverage in width and depth. As they are obtained from ship-based observations, the disadvantage of water column data is that their measurements happened in a certain year and were never repeated.

In our model, we use phosphate data as model simulated dissolved inorganic nutrients ( $C_{Dd}$ ) instead of carbon products from water column data because of the existing amount of phosphate data. There are hundreds of times more phosphate data than carbon data, so that it is possible to have phosphate climatology monthly product. In the upper 500 m of the ocean, they have good data coverage in a one-degree latitude-longitude grid of annual mean as well as climatology monthly. But most depths deeper than 500 m are lacking of data for climatology monthly. In addition, only annual mean phosphate data are available. Due to the stability of the deeper ocean, the monthly variation of phosphate concentrations in deep-ocean are slight, so we take the annual mean phosphate as the climatology monthly data. We take the WOA09 phosphate standard error as the data error  $\sigma_{C_{Dd}}$  with a limited lower boundary of  $0.03 \mu\text{mol kg}^{-1}$  (smaller errors are not trustable, also avoid infinitive values when inversed). This value is used for smaller errors as well as missing errors.

## 2.2 Satellite POC data

In ocean color reprocessing 2009, POC was released as a new remote sensing product according to the new satellite retrieval algorithm (Stramski et al., 2008) (downloaded from <http://oceancolor.gsfc.nasa.gov/cgi/l3>). The POC data used in our present study were measured by the satellite sensor SeaWiFS carried by the SeaStar satellite.

## Assimilating water column and satellite data

X. Yao and R. Schlitzer

Title Page

Abstract

Introduction

Conclusions

References

Tables

Figures

⏪

⏩

◀

▶

Back

Close

Full Screen / Esc

Printer-friendly Version

Interactive Discussion



SeaWiFS is Sea-viewing Wide Field-of-view Sensor, which began scientific operations on 18 September 1997 and stopped collecting data on 11 December 2010. It has 10 yr of continuous observations of the Earth's biological, ecological, and chemical response to climate change. The release of satellite POC data is a big new achievement to monitor the surface water with unprecedented spatial and temporal coverage, which gives a new opportunity for carbon research. Researchers can use directly carbon-related data POC to estimate carbon export instead of estimating carbon export indirectly from chlorophyll.

Satellite POC data have a much better temporal evolution and a higher spatial resolution than water column data. As mentioned before, the water column data were mostly measured in a certain year and most of them never repeated at the same location. While the satellite monitors the ocean surface frequently, it provides continuous temporal POC data. So it is very important to have these satellite data to fill up the gaps of the water column data. Furthermore, SeaWiFS POC data have the spatial resolution of  $9 \times 9$  km, which is much higher than that of water column data. In Fig. 3, the map shows that the SeaWiFS POC data have good coverage of the global ocean and they can provide high-resolution monthly products. In the subtropical gyre, POC concentration is low, while it is higher in the polar region. Because subtropics are warmer than the polar region, they are better for the particles' remineralization. The lack of coverage in polar regions is due to light limitation in September. So satellite POC has the advantage of higher temporal and spatial resolution over water column data. However, because of the limitation of remote sensing, the derived POC is only representative to the top optical depth of the water column, which refers to a few meters in coastal waters and 15–50 m in oceanic waters. So it is hardly possible to have subsurface information. Considering the advantage and disadvantage of satellite POC and water column data, the combination of these two data gives us a full overview of carbon information of the global ocean. Based on satellite and water column data, we present a data assimilation approach that aims at estimating the export of POC in the world ocean at monthly resolution.

---

## Assimilating water column and satellite data

X. Yao and R. Schlitzer

---

[Title Page](#)[Abstract](#)[Introduction](#)[Conclusions](#)[References](#)[Tables](#)[Figures](#)[⏪](#)[⏩](#)[◀](#)[▶](#)[Back](#)[Close](#)[Full Screen / Esc](#)[Printer-friendly Version](#)[Interactive Discussion](#)

As the amount of phosphate water column data has a factor of hundreds more than carbon data, our model is calculated in phosphor unit. Therefore, before using the satellite POC data in the model, it is required to convert carbon to phosphor, using a fixed uniform Redfield ratio ( $C:P = 106$ ) to convert carbon to phosphor. Thus POC is converted to particulate organic phosphorous (POP). We note POP as  $C_{Pd}$  in our model. The converting of POC does not cause any feature changes but only their values are scaled. The feature of POP still follows the pattern of Fig. 2. Currently the accuracy of satellite POC we used in our model is 30 % of the data (private conversation with Stramska, 2010) with a lower boundary of  $12.95 \text{ mgm}^{-3}$  (Stramski et al., 2008). Using the same Redfield ratio we generate the satellite POP error  $\sigma_{C_{Pd}}$  at the meantime.

### 3 Model

The model used in our study is an extension of the adjoint model of Schlitzer (2007). The general model strategy is described in detail in Schlitzer (1993, 1995, 2000, 2002). In the original model, all the tracers are in steady state except CFC. Following the example of CFC, we set up the model with phosphate and POP as model tracers. Phosphate and POP are simulated monthly, and their budgets contain the particle export production parameters, which are used for carbon export estimations.

#### 3.1 Model grid

The model is global and has a non-uniform grid with horizontal resolution ranging between  $1 \times 1^\circ$  and  $4 \times 5^\circ$  (Fig. 3). Finer resolution is realized near coastal regions while coarser resolution prevails in the open ocean. The model has 2421 oceanic columns and three boundary columns adjacent to the Mediterranean Sea, the Red Sea, and the Persian Gulf. The model has 26 vertical layers, with thickness progressively increasing from 60 m at the surface to 500 m at 5000 m depth. Figure 4 shows the main processes in the model. The model has a steady-state 3-D circulation field that was obtained by

fitting the model to a large set of tracer data including CFC and natural radiocarbon (C14) (Schlitzer, 2007). The capability to closely observe CFC and C14 distributions suggests that water mass transport as well as ventilation and overturning rates in the model are realistic. The model includes biological production of suspended as well as sinking particles in the top two layers (euphotic zone; 0–133 m depth). Sinking particles are remineralized in the water column or at the sea floor. More details of the biogeochemical processes in the model follow below.

### 3.2 Model budgets equations

In our study, there are two budgets, inorganic nutrient phosphate  $C_D$  and organic particles POP  $C_P$ . The  $C_D$  and suspended  $C_P$  are coupled in the surface layer (see Fig. 4). During the production process,  $C_D$  is consumed to build up  $C_P$ , while  $C_P$  uses up during the remineralization process, leading to  $C_D$  enrichment. The  $C_D$  budgets exist over the entire water column, and suspended  $C_P$  budgets only exist in the surface layer, sinking  $C_P$  is remineralized over the water column while sinking downward.

The box-wise inventory of  $C_D$  varies with time. The  $C_D$  concentrations are transported by circulation and also affected by biogeochemical processes, PP and particles remineralization. As suspended  $C_P$  biomass particles is formed during phytoplankton photosynthesis near the surface ocean, the material exchange of  $C_D$  and suspended  $C_P$  only happens in the surface layer. The time variation of suspended  $C_P$  is formulated in a way of bulk material exchanges due to source and sink of individual box interior, in order to avoid building up the fully food web. In our model, suspended  $C_P$  is assumed to be referring to satellite monitored organic particles. The sinking part of  $C_P$  is parameterized in the export production parameter.

## Assimilating water column and satellite data

X. Yao and R. Schlitzer

Title Page

Abstract

Introduction

Conclusions

References

Tables

Figures

◀

▶

◀

▶

Back

Close

Full Screen / Esc

Printer-friendly Version

Interactive Discussion





coefficient along depth and guarantees its continuity. This enhancement vanishes at the bottom of MLD.

$q_D$  means the net particle flux getting from the upper box and exporting to the lower box due to particle remineralization. The vertical particle flux  $j_p(z)$  is assumed to follow so-called Martin curves (Martin et al., 1987). It describes the particle flux variation along depths. Production of particulate material occurs in the top two model layers (euphotic zone). The euphotic zone  $z_{EZ}$  is 133 m. Sinking particles are remineralized below the euphotic zone, and the particle flux decreases according to

$$j_p(z) = a \cdot (z/z_{EZ})^{-b} \quad (3)$$

In Eq. (3), the exponent  $b$  determines the shape of the particle flux profile and thus controls the depth of remineralization. Here we use  $b$  values provided by Schlitzer (2007).

The parameter  $a$  represents the particle flux at the depth of the euphotic zone, commonly referred to as export production.

The  $C_P$  budget Eq. (2) is a box-wise budget;  $q_p$  is the interior source and sink. Due to different source and sink, there are two schemes of  $C_P$  budget. One scheme relates the source term to the particle flux at the euphotic zone and the sink term to the particles' decay with time. The other scheme relates the particles' source term to the net primary production (NPP) and the sink term to the particles' remineralization.

According to different strategies of dealing with the source and sink terms, there are two experiments.

The first experiment A (Exp A) of  $C_P$  budgets is:

$$V \frac{dC_P}{dt} = \alpha \cdot a - V \frac{C_P}{\tau} \quad (4)$$

The source term of  $C_P$  is proportion to export production  $a$ , with a proportion factor  $\alpha$ . The export production  $a$  is a value with a fixed prescribed time variation phase; see Eq. (5). The sink term is determined by the decay of  $C_P$  in time scale  $\tau$ .

$$a = \alpha_0 \cdot p_e^2(x, y) \cdot s(y, t) \quad (5)$$

## Assimilating water column and satellite data

X. Yao and R. Schlitzer

Title Page

Abstract

Introduction

Conclusions

References

Tables

Figures

⏪

⏩

◀

▶

Back

Close

Full Screen / Esc

Printer-friendly Version

Interactive Discussion



## Assimilating water column and satellite data

X. Yao and R. Schlitzer

Title Page

Abstract

Introduction

Conclusions

References

Tables

Figures

◀

▶

◀

▶

Back

Close

Full Screen / Esc

Printer-friendly Version

Interactive Discussion



where  $\alpha_0 \cdot p_e^2(x, y)$  is the export flux of the steady state at longitude  $x$  and latitude  $y$ ,  $s(y, t) = 1 + \kappa(y) \cdot \sin(\Phi(y) + 2\pi t)$  is the season factor which is a simplistic empirical formula according to common knowledge,  $t$  is time (in decimal years),  $\kappa(y)$  is the relative amplitude of the seasonal export variations ranging between 0 (no seasonal variations) and 1 (maximal seasonal variations), which has the formula of 4th order of polynomial, and  $\Phi(y)$  is the phase determining the time of maximal export (blooms), which has the formula of 2nd order of polynomial. The coefficients of polynomial are chosen empirically.

In the model, this season factor  $s(y, t)$  is prescribed and fixed for every month.  $p_e^2(x, y)$  is the magnitude of export flux, which can be adjusted in the adjoint model. The reason of its square is to guarantee positive export flux.

The second experiment B (Exp B) of  $C_p$  budgets is:

$$V \frac{dC_p}{dt} = \beta \cdot N_p \cdot A_i - V \cdot \gamma \cdot C_p \quad (6)$$

Here  $N_p$  stands for NPP. In Eq. (6), we relate the  $C_p$  source term proportional to NPP. As NPP is defined for the whole euphotic zone, and the model  $C_p$  budget only exists in the first layer, we assume that  $\beta$  percent of NPP is produced in the first layer. In the model, it is formed as  $p_\alpha^2$ . The value of  $\beta$  varies with the independent parameter  $P_\alpha$ , which could be adjusted in the adjoint model. This NPP product (Behrenfeld and Falkowski, 1997a) is downloaded from the Ocean productivity webpage (<http://orca.science.oregonstate.edu/1080.by.2160.monthly.hdf.vgpm.s.chl.a.sst.php>). And we take 10 % of maximum NPP data to fill up the missing data area of polar regions.

In Eq. (6), the sink term is the  $C_p$  remineralization influenced by water temperature. The remineralization rate  $\gamma$  is formed by a constant value  $p_\gamma^2$  times a temperature dependent factor  $Q$ . In the model, the value of  $p_\gamma$  can be adjusted. The remineralization rate  $\gamma$  is influenced by a temperature factor  $Q$ , which is formed in accordance with Eppley (1972). It is a function of temperature  $Q = G(T(t))$ . The monthly temperature

$T(t)$  data are originally from WOA09 temperature (Locarnini et al., 2010) climatology monthly data.

### 3.3 Model Parameters

In the model, we have two groups of parameters. One group is independent parameters noted as  $\rho^*$ . It is independent of model simulation, but can be adjusted in the adjoint model. It appears in model budgets as parameter. The other group is dependent parameters noted as  $\tilde{\rho}$ . It depends on independent parameters  $\rho^*$ . Different values of independent parameters influence the values of dependent parameters by calculating the budgets equations.

Independent parameters:

$$\begin{aligned} \rho^* &= [\rho_e] && \text{for Exp A} \\ \rho^* &= [\rho_e, \rho_\gamma, \rho_\alpha] && \text{for Exp B} \end{aligned} \quad (7)$$

The set of independent parameters contains three different types, export-independent parameter  $\rho_e$ , remineralization-independent parameter  $\rho_\gamma$  and primary production percentage independent parameter  $\rho_\alpha$ . According to different model strategies, Exp A and Exp B have different numbers of independent parameters. They are all assigned to the model column and have the same size of column number.

In Exp A,  $\rho_e$  is the only independent parameter. It shows up not only in the source and sink term  $q_D$  of  $C_D$  budgets, but also in the source term  $a$  of  $C_P$  budgets. So in Exp A, the varying of the export-independent parameter  $\rho_e$  influence both  $C_D$  and  $C_P$  budgets. The initial value of  $\rho_e$  is gained from Schlitzer's (2007) steady-state model, and it is adjusted in the model adjoint part. This export-independent parameter  $\rho_e$  varies spatially in the global ocean and has the same number of model column 2421. Both water column and satellite data play a role for the adjustment of this export-independent parameter  $\rho_e$ . Model simulation should approach the water column and the satellite data at the same time by adjusting the same independent parameter  $\rho_e$ .

## Assimilating water column and satellite data

X. Yao and R. Schlitzer

Title Page

Abstract

Introduction

Conclusions

References

Tables

Figures

◀

▶

◀

▶

Back

Close

Full Screen / Esc

Printer-friendly Version

Interactive Discussion



In Exp B, besides  $p_e$  there are two additional independent parameters  $p_\gamma$  and  $p_\alpha$ .  $p_\gamma$  is the remineralization-independent parameter to compose parameter  $\gamma$  in Eq. (6). It starts with a globally uniform constant initial value  $p_\gamma^2$  and equals to 0.048 /day (Schartau and Oschlies, 2003). In the model adjoint part, it will be adjusted according to the model grid automatically and individually.  $p_\alpha$  is the primary production percentage independent parameter which composes parameter  $\beta$  in Eq. (6). It starts with a globally uniform value  $p_\alpha^2$  equals to 0.75. In the model adjoint part, it will be also adjusted automatically and individually according to the model grid. All of the independent parameters can only be adjusted spatially in the model and have the fixed value, without any temporal changes. Therefore, in Exp B plus the number of independent parameter  $p_e$  we have a system of 7263 independent parameters in the model. In principle, these 7263 parameters can be adjusted by the model individually in order to fit the observational water column and satellite data.

Dependent parameters:

$$\tilde{p} = [C_D, C_P] \quad (8)$$

The number of dependent parameters is decided by model budgets. There are two budget equations  $C_D$  and  $C_P$ . The size of dependent parameter matrix is decided by the number of  $C_D$  boxes and  $C_P$  boxes and model time steps. As  $C_D$  budgets exist in the whole depth while  $C_P$  budgets only exist in the first surface layer, the amount of  $C_D$  is much more than the number of  $C_P$ . So it is 44388  $C_D$  boxes and 2421  $C_P$  boxes. We calculate  $C_D$  and  $C_P$  budgets in a ten years period with one month time step.  $C_D$  starts from former model results (Schlitzer, 2007) as initial values, while  $C_P$  starts from zero. A ten years period is enough for getting equilibrium and in the ability of machine calculation. The more time steps run, the closer  $C_D$  and  $C_P$  get to observations. So we take the last year's 12 month results of  $C_D$  and  $C_P$  for calculating cost function. This calculating  $C_D$  and  $C_P$  part is called forward run (also called simulation; see Fig. 5) because of its way of time stepping from the first time step to the last one.

### 3.4 Cost function

Once  $C_D$  and  $C_P$  are calculated during the model forward run, the last 12 steps' values of  $C_D$  and  $C_P$  are stored to compare with observations; then they form the cost function  $F$ . The individual terms of cost function are listed in Table 2. The total cost function  $F$  is the sum of all the terms listed.

There are five terms of cost functions in our model. The first four are representing misfits between model-simulated and observational concentrations. The terms 1, 2 and 3 are from calculating misfits between  $C_D$  and water column phosphate data  $C_{Dd}$ . They are divided into three parts, phosphate in surface (< 60 m), shallow water (60 to 400 m) and phosphate in deeper water (> 400 m). Separate terms in cost function allow for a more flexible setting in the model adjoint part. This allows the model to focus on surface, shallow, and deep water phosphates individually. Term 4 calculates the misfits between  $C_P$  and satellite data  $C_{Pd}$ . Term 5 is a horizontal smoothness of export production. The treatment of this smoothing term avoids abrupt changes of export between adjacent regions.

Term 1 to 4 contain the data error  $\sigma_{C_{Dd}}$  and  $\sigma_{C_{Pd}}$ . We take  $\sigma_{C_{Dd}}$  from WOA09. For the missing value area we take  $0.03 \mu\text{mol kg}^{-1}$ . And when the values are smaller than  $0.03 \mu\text{mol kg}^{-1}$  we also take  $0.03 \mu\text{mol kg}^{-1}$ . As there are large amount of missing and invalid data, the average of  $\sigma_{C_{Dd}}$  is  $0.03 \mu\text{mol kg}^{-1}$  for the surface ocean, the shallow ocean and the deep ocean. For  $\sigma_{C_{Pd}}$  we take 30 % of the satellite POC data with a lower bound of  $12.95 \text{ mg m}^{-3}$ . Reldfield ratio is used to convert this POC to POP, and satellite unit  $\text{mg m}^{-3}$  is converted to model unit  $\mu\text{mol kg}^{-1}$  (the ocean density used here is  $1025 \text{ kg m}^{-3}$  and the relation between mol and gram, 1 mol carbon equals to 12 gram). When the misfits between model simulations and observational data are calculated, data errors are taken into account. The cost function term can be very large when the error is very small, leading to a large magnitude in the cost function. This means that the more accurate the observation data are, the more significant values will hold in cost function. This significance will be captured by the adjoint model.

Besides, there are additional terms called weight factor to adjust the magnitudes of different cost function terms. In the model, there are five weight factors multiplying on individual cost function terms to make these five cost function terms to be a dominant term individually. Large weight factor multiplies on the most interesting term, in order to create the dominant term. Once it became a dominant term, the model pursues to achieve the decrease of this term firstly. The weight factors on individual terms for Exp A and Exp B are listed in Table 2.

### 3.5 Adjoint equations

The mathematics of the adjoint model is to find the minimum of cost function under the condition of fulfilling model budgets. First reorder the model budgets  $C_D$  and  $C_P$ , Eqs. (1) and (4) for Exp A while Eqs. (1) and (6) for Exp B, in the homogenous form  $E_j = 0, j = 1, \dots, n_e$ . Form the cost function  $F$ , then write the Lagrangian function  $L$  of the model using cost function and model budgets,

$$L(p^*, \tilde{p}, \lambda) = F(p^*, \tilde{p}) + \sum_{j=1}^{n_e} \lambda_j \cdot E_j \quad (9)$$

Here  $n_e$  means the number of equations,  $\lambda$  is the Lagrange multiplier.

Seeking the minimum of cost function  $F$  is equivalent to finding a model solution that satisfies Eqs. (10), (11) and (12).

$$\frac{\partial L}{\partial \lambda_j} = E_j = 0 \quad (10)$$

$$\frac{\partial L}{\partial \tilde{p}_i} = \frac{\partial F}{\partial \tilde{p}_i} + \sum_{j=1}^{n_e} \lambda_j \cdot \frac{\partial E_j}{\partial \tilde{p}_i} = 0 \quad (11)$$

$$\frac{\partial L}{\partial p_i^*} = \frac{\partial F}{\partial p_i^*} + \sum_{j=1}^{n_e} \lambda_j \cdot \frac{\partial E_j}{\partial p_i^*} = 0 \quad (12)$$

## Assimilating water column and satellite data

X. Yao and R. Schlitzer

Title Page

Abstract

Introduction

Conclusions

References

Tables

Figures



Back

Close

Full Screen / Esc

Printer-friendly Version

Interactive Discussion



As Eq. (10) is automatically fulfilled by  $E_j = 0$  in the model because of the structure of budgets equations. So firstly we solve the Eq. (11) to calculate all the Lagrange multipliers  $\lambda_j$ . Ideally the minimum of cost function  $F$  will be found when Eq. (12) fulfilled, but in numerically we search for a point close to this minimum. In order to get close to this minimum point, we calculate the gradient of the Lagrange function respect to independent parameters with the calculated Lagrange multipliers  $\lambda_j$  substitute in Eq. (12), and find out a descent direction of this gradient by using the decedent algorithm.

This adjoint model applies after simulation as shown in Fig. 5. It is one of the data assimilation techniques. In classical model simulation, there is no such part. The advantage of having this adjoint part is that we can tune model parameters more efficiently. In a classical model, when they want to have more realistic model simulations, they usually tune all possible parameters in the model to have better simulations. Sometimes it can costs lots of tries. However, using adjoint model, we can avoid these inefficient and time-consuming tuning work. These misfits between simulated tracer concentration and observations will be automatically taken into account in the adjoint model. Furthermore, it derives independent parameters' adjustments and leads to more realistic simulations. The tuning of parameters will be automatically done by the model with the knowledge obtained from misfits instead of doing it manually. It is more efficient compared to tuning parameters manually.

As show in Fig. 5, the adjoint model costs the same computing time as the simulation; so in total it costs twice the machine time to finish one whole loop. We call this whole loop iteration. This iteration will be done many times, and it only stops when it fulfills our optimal criteria. The consuming of the machine is only caused by the number of iterations. Our present model is done by a normal PC.

In our study, the Fortran codes of the adjoint model are obtained from the forward model manually by analyzing the matrix used in Eqs. (10) to (12). Besides doing it manually, people also can use automatic Adjoint Model Compilers (Giering and Kaminski, 1998, 2000; Giering et al., 2005).

## 4 Model experiments

The model calculation can be divided into two parts as Fig. 5 shows. The first part is a normal forward-run model, same as any classical model simulation in our study, solving the budget equations with initialized independent parameters and solving the  $C_D$  and  $C_P$  field implicitly. The other part of the model is the adjoint model, which compares the simulated  $C_D$  with the water column  $C_{Dd}$  data and the simulated  $C_P$  with the satellite  $C_{Pd}$  data by calculating their misfits. The knowledge on independent parameters' improvement is gained from these misfits in the adjoint model, and then improved by utilizing independent parameters in the simulation again. This loop will be repeated many times until it fulfills our optimal criteria when the model simulations are closer enough to observations by tracking the values of cost function. This adjoint model guarantees that the next iteration simulation with improved model parameters will have better  $C_D$  and  $C_P$ , which means closer to the observations than previous simulation.

In our study, we have done two different experiments, Exp A and Exp B. One uses Eqs. (1) and (4). It is an export production based experiment (Exp A). The other uses Eqs. (1) and (6); it is an NPP based experiment (Exp B). By solving the budgets equations, we use an implicit differencing scheme in time that allows large time steps. So we use one month time step, and in order to get equilibrium in the model we run it in a ten years period. The initial values of  $C_D$  come from steady state model results (Schlitzer, 2007), and  $C_P$  initial values are zero. By solving the budgets equations with one month time step in a ten years period, we can store the complete history (120 time steps) of  $C_D$  and  $C_P$  concentrations in memory for the usage in the subsequent adjoint run. Using the last year's 12 month  $C_D$  and  $C_P$  concentrations minus  $C_{Dd}$  and  $C_{Pd}$  individually, divided by the data errors and then squared, we form the cost function term of  $C_D$  and  $C_P$  as listed in Table 2. The monthly calculation of cost function represents the annual mean of the cost function. Adding the contribution of export production smoothness forms the total cost function. We start the adjoint model with a backward time

# GMDD

6, 2045–2085, 2013

## Assimilating water column and satellite data

X. Yao and R. Schlitzer

Title Page

Abstract

Introduction

Conclusions

References

Tables

Figures

⏪

⏩

◀

▶

Back

Close

Full Screen / Esc

Printer-friendly Version

Interactive Discussion



## Assimilating water column and satellite data

X. Yao and R. Schlitzer

Title Page

Abstract

Introduction

Conclusions

References

Tables

Figures

⏪

⏩

◀

▶

Back

Close

Full Screen / Esc

Printer-friendly Version

Interactive Discussion



stepping, solving the time step from the last to the previous ones. With the backward time stepping and special structure of matrix of Eq. (11), we get a benefit of solving all the Lagrange multipliers  $\lambda_j$  with setting Eq. (11) to zero, then put  $\sum_{j=1}^{n_e} \lambda_j \cdot \frac{\partial E_j}{\partial \bar{p}_i}$  to the right hand side. Using these known values of  $F$ , we solve unknown Lagrange multipliers  $\lambda_j$ . Then substituting the solved Lagrange multipliers  $\lambda_j$  into Eq. (12), we calculate the gradient of the Lagrange function  $L$  with respect to independent parameters  $p^*$ . Once we have calculated the gradient of the Lagrange function with respect to independent parameters, descent algorithm (quasi-Newton conjugate gradient algorithm) plays a role. It will find a descendent direction of the gradient, then go one step further from the independent parameters along this direction. Then with the new independent parameters, it will start the simulation again. This iteration will repeat many times in order to get a descent of the gradient and to pursue to find the minimum of cost function.

Like the different number of independent parameters of Exp A and Exp B, the matrix size of Eq. (11) is different. Exp B needs to calculate two more gradients for the additional independent parameters  $p_\gamma$  and  $p_\alpha$ . So Exp B costs more computer time.

## 5 Results and discussion

### 5.1 Cost function values

The present study contains two different experiments, Exp A and Exp B. Both experiments used the same constraints as listed in Table 2. Exp A and Exp B have been run with the weight factors listed in Table 2. The results of cost function indicate the descent of cost function as the model iterates. Both the total cost function and individual terms are shown in Table 3. Large values exist in two terms, the phosphate (< 60 m) term and the satellite POC term (Redfield ratio is used again to convert POP to POC in the model result outputs). The difference of starting values of the satellite POC term, in Exp A and Exp B, is caused by using different  $C_p$  budgets. The difference of the phosphate (< 60 m) term is caused by particles remineralization in the first layer.

## Assimilating water column and satellite data

X. Yao and R. Schlitzer

Title Page

Abstract

Introduction

Conclusions

References

Tables

Figures

⏪

⏩

◀

▶

Back

Close

Full Screen / Esc

Printer-friendly Version

Interactive Discussion



The values of total cost function show the decreasing, Exp A is reduced by 12 % and Exp B is reduced by 95 %. Obviously, Exp B decreases more than Exp A, although Exp B has a larger starting value. Exp B reaches a smaller cost function than Exp A at the end. In Exp A, the main contribution of the decreasing comes from the satellite POC term, reduced by 75 %, and it is hard for phosphate cost functions terms to decrease. In Exp B, the phosphate (< 60 m) term is reduced by 52 % and the satellite POC term is reduced by 99 %.

Compared to Exp B, Exp A is much harder to get reduced both in the phosphate (< 60 m) term and the satellite POC term. In Exp A, the export production independent parameter  $p_e$  is the only adjustable parameter, and its adjustment directly influences the surface POC and the phosphate. When the adjoint model searches for a descent direction of cost function, it needs to consider the misfits of both phosphate and POC. It is difficult to get a point that can reduce both of them. In this case it is a competition of phosphate and POC. The stronger the weight factor is the more powerful cost function has on influencing the direction of decreasing. In the end, it decides to decrease the misfits of POC. This difficulty is also caused by the disagreement of phosphate and POC data under our current model set up. The mathematically described relation between phosphate and POC is conflicted with the data themselves. This becomes a barrier for the descent in the adjoint model. However, in Exp B there is no such restriction. There are two more additional independent parameters  $p_\alpha$  and  $p_\gamma$  to be adjusted to fit the surface POC. It has more freedom than Exp A in the adjoint model. This is the reason why Exp B can reduce the cost function more strongly than Exp A.

## 5.2 Misfit analysis

Based on the model solutions of POC and phosphate, we calculate their mean misfits and the RMSs (root mean square), they are listed in Table 4. Exp B shows smaller POC misfits and RMS than Exp A. Both Exp A and Exp B show that the model simulation has underestimated POC concentrations in general.

## Assimilating water column and satellite data

X. Yao and R. Schlitzer

Title Page

Abstract

Introduction

Conclusions

References

Tables

Figures

⏪

⏩

◀

▶

Back

Close

Full Screen / Esc

Printer-friendly Version

Interactive Discussion



The annual phosphate mean misfits and RMSs are listed in three groups, surface layer (< 60 m), shallow water (60 m to 400 m), and deep water (> 400 m). Exp B phosphate has smaller values than Exp A in the surface layer. This is consistent with the smaller value of the phosphate (< 60 m) cost function term of Exp B. The phosphate misfit of Exp B is larger than that of Exp A in shallow water. And no difference is shown in deep water, because of the slight influence on the phosphate (> 400 m) cost function term.

Overall, Exp B has better interpreted the satellite POC and surface phosphate water column data. Two more additional independent parameters in the adjoint model make Exp B work better than Exp A in the aspect of the surface region. It is worth to introduce more independent parameters, although it costs more computation time.

### 5.3 Surface phosphate and POC analysis

Figure 6 shows the model-simulated phosphate field of June and December. The simulated phosphates follow the main structure of WOA09 phosphate, with low concentrations in the subtropic regions and high concentrations in the subpolar regions. In Exp A, there are negative concentrations in the Atlantic subtropics. This is not realistic because of the scarification of the adjoint model in terms of fitting POC data. In Exp B, these unrealistic regions vanished, because the fitting of phosphate is more independent in the adjoint model and performs better than Exp A. In Fig. 6b and d, we see more red in the Pacific Ocean and in the high latitudes of the North Atlantic compared to Fig. 6f and 6h. In Exp A, the concentrations in these regions are more overestimated than Exp B. There is more blue in the Atlantic, which shows more underestimating in Exp A. In general, the adjoint model works better in Exp B than in Exp A in the aspect of fitting water column phosphate data.

Figure 7 shows the model-simulated POC field of June and December. Significant differences are shown both in Exp A and Exp B. In Exp A, the POC concentrations are underestimated in most regions in June and December. They are more overestimated in the southern ocean region in December compared to June. Figure 7a and b show

## Assimilating water column and satellite data

X. Yao and R. Schlitzer

Title Page

Abstract

Introduction

Conclusions

References

Tables

Figures



Back

Close

Full Screen / Esc

Printer-friendly Version

Interactive Discussion



a slightly seasonal shift of overestimated regions, and it is related to seasonal changes of productivity. In Exp B, there is less blue and red than in Exp A. But it is still showing the seasonal shift of overestimated regions, June in the northern ocean and December in the southern ocean. Exp B has better simulated the POC concentrations in the sub-tropics. The results show a better simulation in the subtropical region and a worse one in the polar region, which can be the reason for more missing data in the polar region. Due to light limitation and satellite coverage, the polar region often lacks satellite observation. Without observations, the adjoint model cannot work because contributions of cost function in these missing data regions are missing. So the adjoint gains nothing in these regions; it cannot influence the adjustment of independent parameters either. This results in a bad simulation in the polar region.

In Fig. 8a, we choose a point at the mid-latitude of the North Pacific Ocean, where obvious seasonal changes show in Fig. 1. When we focus on the relation of the WOA phosphate and the satellite POC, we find they are not always anti-correlated (see Fig. 8b). From February to March, the POC is increasing, and phosphate is not decreasing. This may be caused by the winter MLD deepening (see Fig. 8e), which brings up the phosphate to the surface. From May to July, phosphate and POC are both decreasing, and phosphate concentration is not affected by the MLD because it is shallower than 60 m. In this period, the relation of POC and phosphate conflicts with their anti-correlated relation in our model set up.

Figure 8c shows the monthly simulated phosphate of Exp A and Exp B. The simulated phosphate concentration of Exp A is higher than the WOA phosphate concentration. The simulated phosphate concentration of Exp B is relatively fitting to the WOA phosphate concentration. In Fig. 8, the simulated POC of Exp B is closer to the satellite POC than the simulated POC of Exp A. This is the reason for better preference of adjoint model of Exp B, there is more freedom in Exp B than Exp A when it chooses the direction of descent.

In Exp A, the adjustment of the export production independent parameter affects the simulation of phosphate as well as POC, whether increase or decrease the phosphate

cost function term or the POC cost function term. Then the choice of descent direction is the competition between the weight of phosphate and POC cost function terms. Usually it is hard for the model to choose a proper export production independent parameter under these constraints, especially when there is a discrepancy of POC and phosphate data. So the existing of a conflicted relation between model setting and observational data influences the ability of the adjoint model.

#### 5.4 POC export analysis

Figure 9 shows the POC export of Exp A and Exp B of June and December. Both Exp A and Exp B show the seasonal changes of the POC export, especially the evolution of high export regions. In June, the high export regions exist in the Northern Hemisphere high latitudes of the North Atlantic, the North Pacific and the east coast of Africa. In December, the highest export regions are in the southern ocean, the coast region of Africa and the southern subpolar regions. The seasonal evolution of high export regions is consistent with the seasonal changes of high productivity. It is decided by rich nutrients, plenty of light and warm temperature. During northern hemispheric summer, the Northern Hemisphere has the proper conditions for high productivity, while during winter the Southern Hemisphere has the better conditions.

By integrating the particle fluxes at the euphotic zone, we calculate the global POC export. The mean global POC export of Exp A is  $9.9 \text{ GtCyr}^{-1}$ , while Exp B is  $12.3 \text{ GtCyr}^{-1}$ . Back to literatures, it suggests that the global POC export production is in the range of 11 to  $22 \text{ GtCyr}^{-1}$  (Laws et al., 2000; Schlitzer, 2000; Eppley and Peterson, 1979). So the value from Exp A relatively underestimates the global POC export. Compared to Exp A, the POC export value from Exp B is more acceptable. This can be the reason for the better explanation of water column and satellite data in Exp B.

## GMDD

6, 2045–2085, 2013

### Assimilating water column and satellite data

X. Yao and R. Schlitzer

Title Page

Abstract

Introduction

Conclusions

References

Tables

Figures

◀

▶

◀

▶

Back

Close

Full Screen / Esc

Printer-friendly Version

Interactive Discussion



## 6 Conclusions

In this study, we use a medium resolution coupled biogeochemical and physical ocean model and assimilate satellite POC as well as water column nutrient data to estimate the seasonal evolution of carbon export in the global ocean. As an extension of previous work, addition of satellite data with their good spatial and temporal coverage allows estimating the temporal variation of the global carbon export fields. The extended model simulates surface water POC concentrations in addition to nutrient concentrations throughout the water column. Both simulated fields are compared with respective observations, and model misfits are accumulated in the cost function of the model. The adjoint method is applied to drive the model to the satellite POC as well as water column nutrient data and to optimize the export production values. Experiments are done using two different POP budget equations (Redfield ration is used to convert POC to POP), which refer to the export production based (Exp A) and to the NPP based (Exp B) experiment. The integrated carbon exports in the two experiments amount to 9.9 (Exp A) and 12.3 GtCyr<sup>-1</sup> (Exp B), respectively. The model results show that the adjoint method worked well with our current model strategy. We also see the descent of cost function, so it does drive the model simulations closer to observations.

In the surface layer, we allow material exchanges between dissolved phosphate and particulate phosphorous POP. The relation between phosphate and POP is anti-correlated. When POP builds up, consuming phosphate, it leads to a decrease in phosphate concentration. When POP is remineralized, dissolved phosphate will be released. Such an anti-correlated relation between the two parameters is also found in the water column and satellite data. However, in some locations and months, this relation is not exactly fulfilled. In these places, we find that the simulated  $C_D$  and  $C_P$  often hardly get closer to each other in both water column and satellite data, and they also influence the surrounding locations. We found in Exp A that the discrepancy of water column and satellite data interferes in driving the model simulations closer to

# GMDD

6, 2045–2085, 2013

## Assimilating water column and satellite data

X. Yao and R. Schlitzer

Title Page

Abstract

Introduction

Conclusions

References

Tables

Figures



Back

Close

Full Screen / Esc

Printer-friendly Version

Interactive Discussion



observations in the adjoint model. In Exp B, the influence of this discrepancy is reduced by introducing two more independent parameters.

However, the existence of significant and systematic differences between model and observations strongly suggests that the treatment of POP budgets and the coupling with dissolved nutrients is overly simplistic and unrealistic. This is especially true for Exp A which exhibits relatively small improvements in the POP fields. While the present study has shown that in principle the adjoint method can be applied for determination of time varying export flux fields using satellite and water column data, the present results have to be considered preliminary and more refined model setups coupling the dissolved and particulate phases of nutrients and carbon are needed.

*Acknowledgements.* The authors thank Ines Borrione for technical support during processing of the satellite data, Ying Ye for discussions on particle-related biological processes in the ocean, and Andrea Bleyer for improving the language of the manuscript. Financial support was provided by the EU FP7 project CARBOCHANGE under grant agreement no. 264879.

## References

- Anderson, L. A. and Sarmiento, J. L.: Redfield ratios of remineralization determined by nutrient data analysis, *Global Biogeochem. Cy.*, 8, 65–80, 1994.
- Aumont, O., Maier-Reimer, E., Blain, S., and Monfray, P.: An ecosystem model of the global ocean including Fe, Si, P colimitations, *Global Biogeochem. Cy.*, 17, 1060, doi:10.1029/2001GB001745, 2003.
- Balch, W., Gordon, H., Bowler, B., Drapeau, D., and Booth, E.: Calcium carbonate measurements in the surface global ocean based on Moderate-Resolution Imaging Spectroradiometer data, *J. Geophys. Res.*, 110, C07001, doi:10.1029/2004JC002560, 2005.
- Behrenfeld, M. J. and Falkowski, P. G.: Photosynthetic rates derived from satellite-based chlorophyll concentration, *Limnol. Oceanogr.*, 42, 1–20, 1997a.
- Bishop, J. K. B. and Wood, T. J.: Year-round observations of carbon biomass and flux variability in the Southern Ocean, *Global Biogeochem. Cy.*, 23, GB2019, doi:10.1029/2008GB003206, 2009.

# GMDD

6, 2045–2085, 2013

## Assimilating water column and satellite data

X. Yao and R. Schlitzer

Title Page

Abstract

Introduction

Conclusions

References

Tables

Figures

◀

▶

◀

▶

Back

Close

Full Screen / Esc

Printer-friendly Version

Interactive Discussion



## Assimilating water column and satellite data

X. Yao and R. Schlitzer

Title Page

Abstract

Introduction

Conclusions

References

Tables

Figures

⏪

⏩

◀

▶

Back

Close

Full Screen / Esc

Printer-friendly Version

Interactive Discussion



Buesseler, K., Pike, S., Maiti, K., Lamborg, C., Siegel, D., and Trull, T.: Th<sup>234</sup> as a tracer of spatial, temporal and vertical variability in particle flux in the North Pacific, *Deep-Sea Res. Pt. 1*, 56, 1143–1167, 2009.

Eppley, R.: Temperature and phytoplankton growth in the sea, *Fish. B-Noaa.*, 70, 1063–1085, 1972.

Eppley, R. and Peterson, B.: Particulate organic matter flux and planktonic new production in the deep ocean, *Nature*, 282, 677–680, 1979.

Garcia, H. E., Locarnini, R. A., Boyer, T. P., Antonov, J. I., Zweng, M. M., Baranova, O. K., and Johnson, D. R.: *World Ocean Atlas 2009, Nutrients (Phosphate, Nitrate, Silicate)*, Vol. 4, edited by: Levitus, S., NOAA Atlas NESDIS 71, US Government Printing Office, Washington DC, 398 pp., 2010.

Gardner, W.: *Sediment Trap Sampling in Surface Waters*, Cambridge University Press, Cambridge, 240–281, 2000.

Giering, R. and Kaminski, T.: Recipes for adjoint code construction, *ACM T. Math. Software*, 24, 437–474, 1998.

Giering, R., Kaminski, T., and Slawig, T.: Generating efficient derivative code with TAF: adjoint and tangent linear Euler flow around an airfoil, *Future Gener. Comp. Sy.*, 21, 1345–1355, 2005.

Gordon, H., Boynton, G., Balch, W., Groom, S., Harbour, D., and Smyth, T.: Retrieval of coccolithophore calcite concentration from SeaWiFS imagery, *Geophys. Res. Lett.*, 28, 1587–1590, 2001.

Gust, G., Michaels, A., Johnson, R., Deuser, W., and Bowles, W.: Mooring line motions and sediment trap hydromechanics: in situ intercomparison of three common deployment designs, *Deep-Sea Res. Pt. 1*, 41, 831–857, 1994.

Honjo, S., Manganini, S. J., Krishfield, R. A., and Francois, R.: Particulate organic carbon fluxes to the ocean interior and factors controlling the biological pump: a synthesis of global sediment trap programs since 1983, *Prog. Oceanogr.*, 76, 217–285, 2008.

Kahler, P. and Bauerfeind, E.: Organic particles in a shallow sediment trap: substantial loss to the dissolved phase, *Limnol. Oceanogr.*, 719–723, 2001.

Laws, E., Falkowski, P., Smith, W., Ducklow, H., and McCarthy, J.: Temperature effects on export production in the open ocean, *Global Biogeochem. Cy.*, 14, 1231–1246, 2000.

Locarnini, R. A., Mishonov, A. V., Antonov, J. I., Boyer, T. P., Garcia, H. E., Baranova, O. K., Zweng, M. M., and Johnson, D. R.: *World Ocean Atlas 2009, Temperature*, Vol. 1, edited by:

## Assimilating water column and satellite data

X. Yao and R. Schlitzer

Title Page

Abstract

Introduction

Conclusions

References

Tables

Figures

◀

▶

◀

▶

Back

Close

Full Screen / Esc

Printer-friendly Version

Interactive Discussion



Levitus, S., NOAA Atlas NESDIS 68, 184 pp., Washington, D.C., US Government Printing Office, 2010.

Martin, J. H., Knauer, G. A., Karl, D. M., and Broenkow, W. W.: VERTEX: Carbon cycling in the Northeast Pacific, *Deep-Sea Res.*, 34, 267–285, 1987.

5 Monterey, G. and Levitus, S.: Seasonal Variability of Mixed Layer Depth for the World Ocean., US Gov. Printing Office, Washington DC, 96 pp., figs p. 87, 1997.

Oschlies, A. and Kähler, P.: Biotic contribution to air-sea fluxes of CO<sub>2</sub> and O<sub>2</sub> and its relation to new production, export production, and net community production, *Global Biogeochem. Cy.*, 18, doi:10.1029/2003GB002094, 2004.

10 Palmer, J. and Totterdell, I.: Production and export in a global ocean ecosystem model, *Deep-Sea Res. Pt. 1*, 48, 1169–1198, 2001.

Redfield, A. C., Ketchum, B. H., and Richards, F. A.: The influence of organisms on the composition of sea-water, in: *The Sea*, edited by: Hill, M. N., Vol. 2, Interscience, New York, 26–27, 1963.

15 Rutgers v. d. Loeff, M., Cai, P., Stimac, I., Bracher, A., Middag, R., Klunder, M., and Van Heuven, S.: Th<sup>234</sup> in surface waters: distribution of particle export flux across the Antarctic Circumpolar Current and in the Weddell Sea during the GEOTRACES expedition ZERO and DRAKE, *Deep-Sea Res. Pt. 2*, 58, 2749–2766, 2011.

Sarmiento, J. and Sundquist, E.: Revised budget for the oceanic uptake of anthropogenic carbon dioxide, *Nature*, 356, 589–593, 1992.

20 Schartau, M. and Oschlies, A.: Simultaneous data-based optimization of a 1-D-ecosystem model at three locations in the North Atlantic: Part I – Method and parameter estimates, *J. Mar. Res.*, 61, 765–793, 2003.

Schlitzer, R.: Determining the mean, large-scale circulation of the Atlantic with the adjoint method, *J. Phys. Oceanogr.*, 23, 1935–1952, 1993.

25 Schlitzer, R.: Applying the adjoint method for global biogeochemical modeling, in: *Inverse Methods in Global Biogeochemical Cycles*, edited by: Kasibhatla, P., Heimann, M., Hartley, D., Mahowald, N., Prinn, R., and Rayner, P., AGU Geophys., Monograph Series, Vol. 114, 2004.

Schlitzer, R.: Carbon export fluxes in the Southern Ocean: results from inverse modeling and comparison with satellite-based estimates, *Deep-Sea Res. Pt. II*, 49, 1623–1644, 2002.

30 Schlitzer, R.: Assimilation of radiocarbon and chlorofluorocarbon data to constrain deep and bottom water transports in the world ocean, *J. Phys. Oceanogr.*, 37, 259–276, 2007.

Stramski, D., Reynolds, R. A., Babin, M., Kaczmarek, S., Lewis, M. R., Röttgers, R., Scian-  
dra, A., Stramska, M., Twardowski, M. S., Franz, B. A., and Claustre, H.: Relationships  
between the surface concentration of particulate organic carbon and optical properties  
in the eastern South Pacific and eastern Atlantic Oceans, *Biogeosciences*, 5, 171–201,  
doi:10.5194/bg-5-171-2008, 2008.

5

Volk, T. and Hoffert, M. I.: Ocean carbon pumps: analysis of relative strengths and efficiencies  
in ocean-driven atmospheric CO<sub>2</sub> changes, the carbon cycle and atmospheric CO<sub>2</sub>: *Natural  
Variations Archean to Present*, Geoph. Monog. Series, 32, 99–110, 1985.

## GMDD

6, 2045–2085, 2013

### Assimilating water column and satellite data

X. Yao and R. Schlitzer

Title Page

Abstract

Introduction

Conclusions

References

Tables

Figures

⏪

⏩

◀

▶

Back

Close

Full Screen / Esc

Printer-friendly Version

Interactive Discussion



## Assimilating water column and satellite data

X. Yao and R. Schlitzer

Title Page

Abstract

Introduction

Conclusions

References

Tables

Figures

◀

▶

◀

▶

Back

Close

Full Screen / Esc

Printer-friendly Version

Interactive Discussion



**Table 1.** The parameters used in the model.

Notation	Meaning	Note
$p^*$	In parameter	
$\bar{p}$	Dependent parameter	
$p_e$	Export independent parameter (Exp A only)	initial value from Schlitzer (2007)
$p_Y$	Remineralization independent parameter (Exp B only)	initial value: $P_Y^2 = 0.048/d$ . (Schartau and Oschlies, 2003)
$p_\alpha$	Primary production percentage independent parameter (Exp B only)	initial value: $P_\alpha^2 = 0.75$
$\alpha$	Proportional factor to export production	
$\tau$	Life time of POP	10 days
$Q$	Temperature factor	(Eppley, 1972)
$b$	Exponent of Martin type particle flux profile	(Martin et al., 1987)
$\beta$	Proportional factor of NPP	$\beta = p_\alpha^2$
$\gamma$	Remineralization rate	$\gamma = p_Y^2 \cdot Q$
$u, v, w$	Zonal meridional and vertical flow	
$C_D$	Phosphate concentration	
$C_{Dd}$	WOA 2009 phosphate concentration	
$\sigma_{C_{Dd}}$	Error of WOA 2009	
$C_P$	Particulate organic phosphorous POP concentration	
$C_{Pd}$	Satellite derived POP concentration	converted from satellite POC using Redfield ratio
$\sigma_{C_{Pd}}$	Error of satellite POP	
$a$	Export production	
$j_p$	Particle flux	
$A$	Area of model box	
$V$	Volume of model box	

## Assimilating water column and satellite data

X. Yao and R. Schlitzer

Title Page

Abstract

Introduction

Conclusions

References

Tables

Figures

⏪

⏩

◀

▶

Back

Close

Full Screen / Esc

Printer-friendly Version

Interactive Discussion



**Table 2.** Cost function  $F$  description of individual terms in the model.

Index	Meaning	Mathematical Form	Weight factor	
			Exp A	Exp B
1	Phosphate data (< 60 m)	$\left(\frac{C_D - C_{Dd}}{\sigma_{C_{Dd}}}\right)^2$	100	100
2	Phosphate data (60–400 m)	$\left(\frac{C_D - C_{Dd}}{\sigma_{C_{Dd}}}\right)^2$	5	5
3	Phosphate data (> 400 m)	$\left(\frac{C_D - C_{Dd}}{\sigma_{C_{Dd}}}\right)^2$	1	1
4	Satellite POC data	$\left(\frac{C_P - C_{Pd}}{\sigma_{C_{Pd}}}\right)^2$	100	100
5	Smoothness of export production in horizontal	Square of second derivative of export production in zonal and meridional	50	50

$\sigma_{C_{Dd}}$  is originally from the WOA09 phosphate standard error with a limit of  $0.03 \mu\text{mol kg}^{-1}$ .  $\sigma_{C_{Pd}}$  is taken 30 % of the satellite POC with a lower bound of  $12.95 \text{ mg m}^{-3}$ .

## Assimilating water column and satellite data

X. Yao and R. Schlitzer

**Table 3.** Values of total cost function and individual terms of the model (in the unit of  $10^7$ ).

		Total cost function	Phosphate (< 60 m)	Phosphate shallow (60–400 m)	Phosphate deep (> 400 m)	Satellite POC term	Smoothness of export production
Exp A	start	35.2	25.3	3.5	0.7	4.0	1.8
	end	31.1	25.3	3.1	0.7	1.0	0.9
Exp B	start	294.9	22.4	3.2	0.7	267.2	1.4
	end	16.2	10.8	3.2	0.8	0.3	1.2

[Title Page](#)
[Abstract](#)
[Introduction](#)
[Conclusions](#)
[References](#)
[Tables](#)
[Figures](#)
[Back](#)
[Close](#)
[Full Screen / Esc](#)
[Printer-friendly Version](#)
[Interactive Discussion](#)


## Assimilating water column and satellite data

X. Yao and R. Schlitzer

Title Page

Abstract

Introduction

Conclusions

References

Tables

Figures

⏪

⏩

◀

▶

Back

Close

Full Screen / Esc

Printer-friendly Version

Interactive Discussion



**Table 4.** Annual RMS of phosphate and POC.

Depth	Exp A		Phosphate ( $\mu\text{mkg}^{-1}$ )		Exp B		Phosphate ( $\mu\text{mkg}^{-1}$ )	
	POC ( $\text{mgm}^{-3}$ )		Mean	RMS	POC ( $\text{mgm}^{-3}$ )		Mean	RMS
	Mean	RMS	Mean	RMS	Mean	RMS	Mean	RMS
Surface layer	-30.85	88.00	0.06	0.31	-8.71	65.87	0.03	0.20
Shallow(60–400 m)	–	–	-0.05	0.28	–	–	-0.08	0.28
Deep(> 400 m)	–	–	0.03	0.13	–	–	0.03	0.14

Here “Mean” refers to mean difference between simulated concentrations and observations, which is model concentrations minus observations.

## Assimilating water column and satellite data

X. Yao and R. Schlitzer

Title Page

Abstract

Introduction

Conclusions

References

Tables

Figures

◀

▶

◀

▶

Back

Close

Full Screen / Esc

Printer-friendly Version

Interactive Discussion

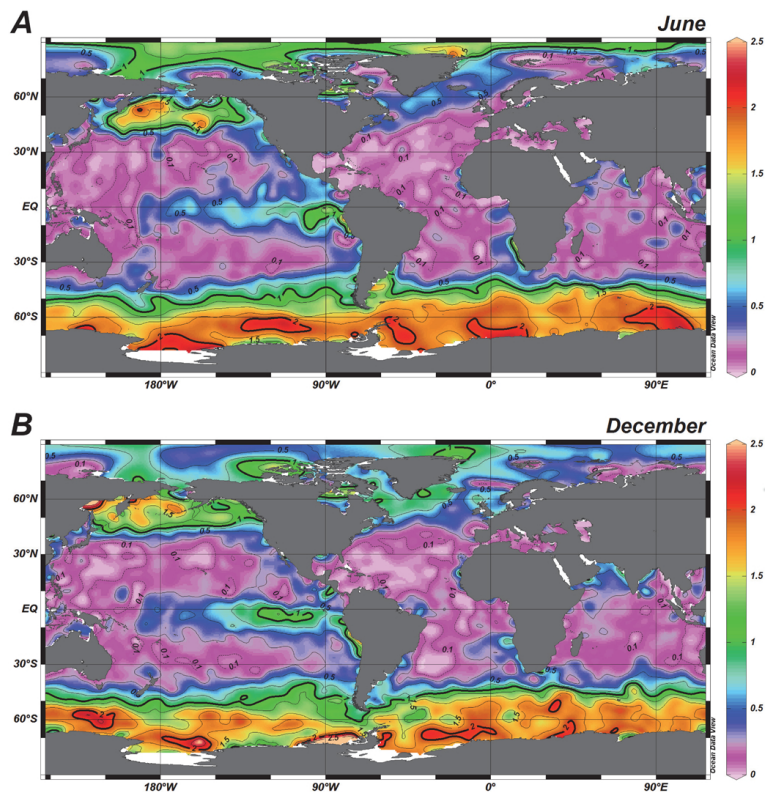


Fig. 1. Phosphate concentrations (unit  $\mu\text{mol L}^{-1}$ ) at 10m of June (A) and December (B).

## Assimilating water column and satellite data

X. Yao and R. Schlitzer

Title Page

Abstract

Introduction

Conclusions

References

Tables

Figures

◀

▶

◀

▶

Back

Close

Full Screen / Esc

Printer-friendly Version

Interactive Discussion

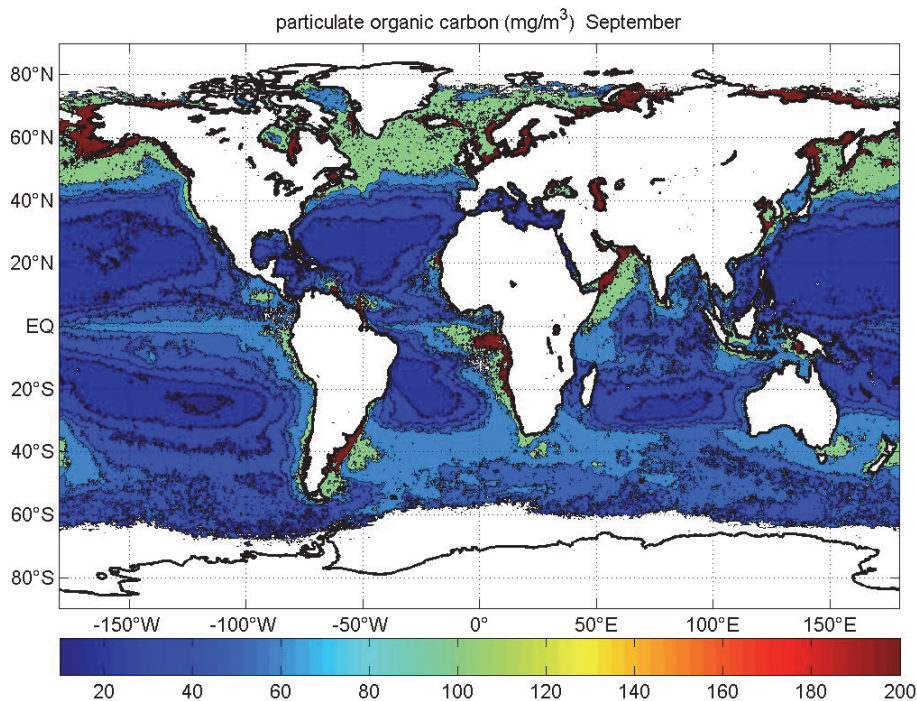


**Fig. 2.** An example of SeaWiFS climatology monthly POC data (September). The unit  $\text{mg}/\text{m}^3$  is converted to  $\mu\text{kg}/\text{m}^3$  in the model by using the ocean density  $1025 \text{ kg}/\text{m}^3$  and the relation between mol and gram; 1 mol carbon equals to 12 gram.

# GMDD

6, 2045–2085, 2013

## Assimilating water column and satellite data

X. Yao and R. Schlitzer

Title Page

Abstract

Introduction

Conclusions

References

Tables

Figures



Back

Close

Full Screen / Esc

Printer-friendly Version

Interactive Discussion

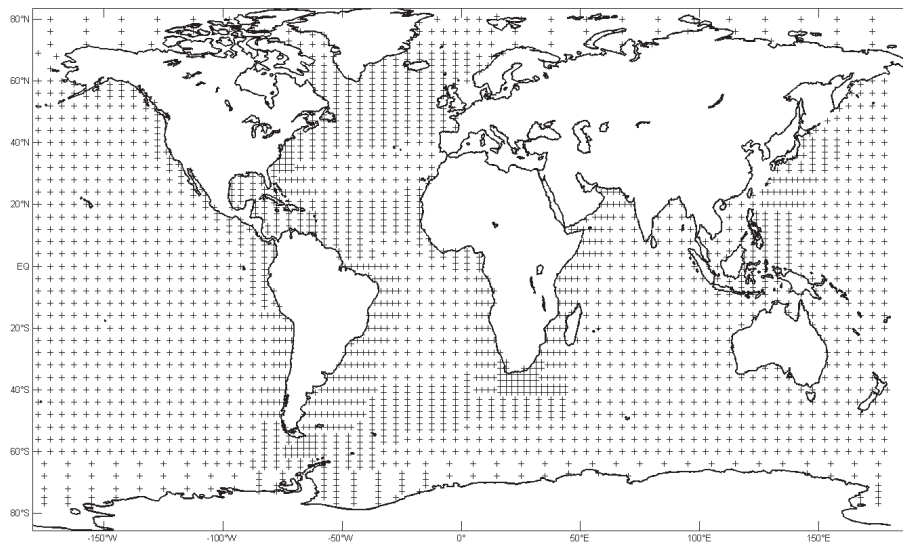


**Fig. 3.** Variable resolution model grid.

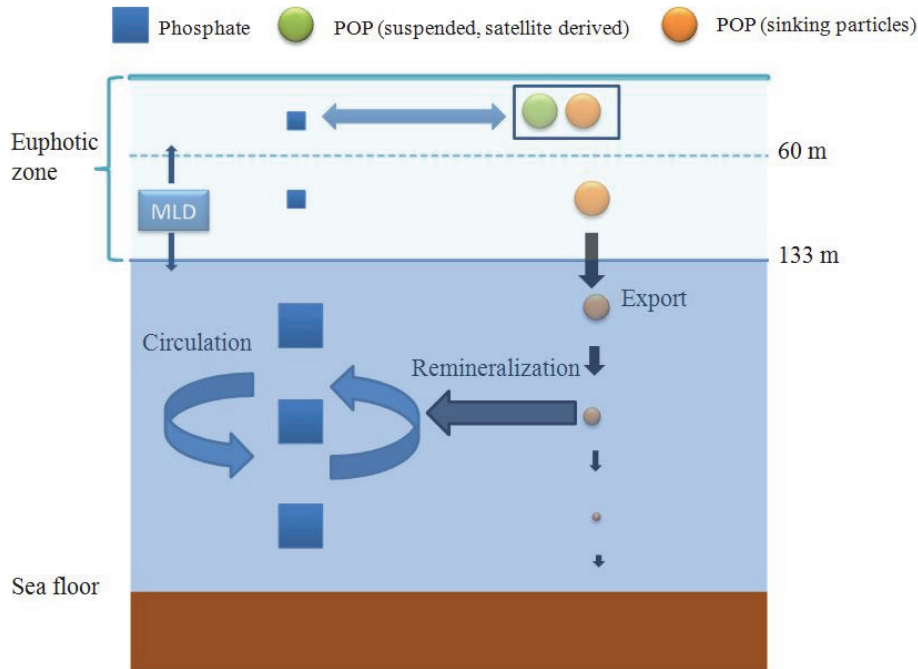


**Fig. 4.** Schematic of model processes. It is a phosphorus unit model, the size of blue square indicates the difference of phosphate concentration between euphotic zone (small) and deep water (big). The size of black arrow indicates the decrease of export. And the size changes of orange circle shows the remineralization process of organic particles under the euphotic zone. The phosphate is transported by the ocean circulation (two big blue arrows) and also influenced by the seasonal changes of mixed layer depth.

**Assimilating water column and satellite data**

X. Yao and R. Schlitzer

Title Page

Abstract

Introduction

Conclusions

References

Tables

Figures

◀

▶

◀

▶

Back

Close

Full Screen / Esc

Printer-friendly Version

Interactive Discussion



## Assimilating water column and satellite data

X. Yao and R. Schlitzer

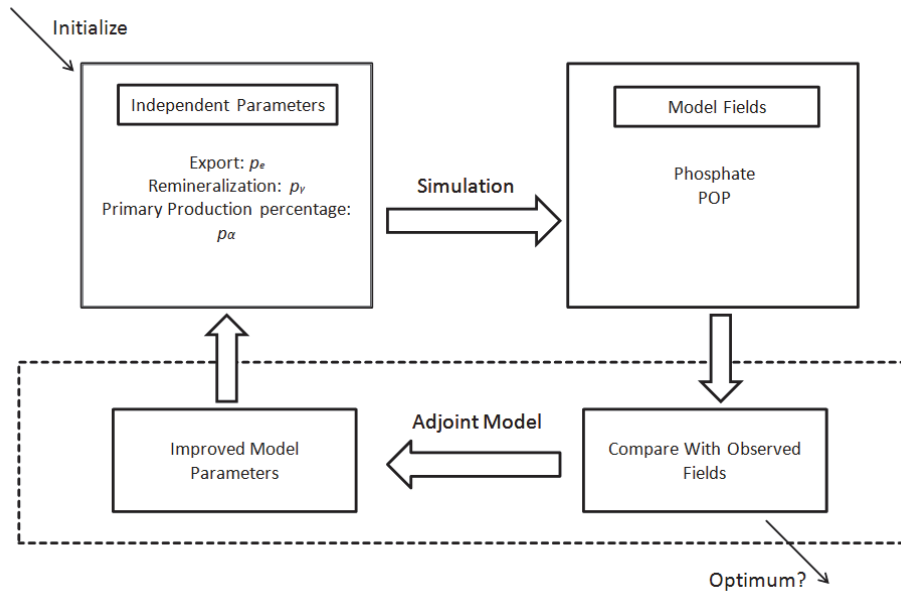


Fig. 5. Schematic overview of model calculations.

Title Page

Abstract

Introduction

Conclusions

References

Tables

Figures

◀

▶

◀

▶

Back

Close

Full Screen / Esc

Printer-friendly Version

Interactive Discussion



## Assimilating water column and satellite data

X. Yao and R. Schlitzer

Title Page

Abstract

Introduction

Conclusions

References

Tables

Figures



Back

Close

Full Screen / Esc

Printer-friendly Version

Interactive Discussion

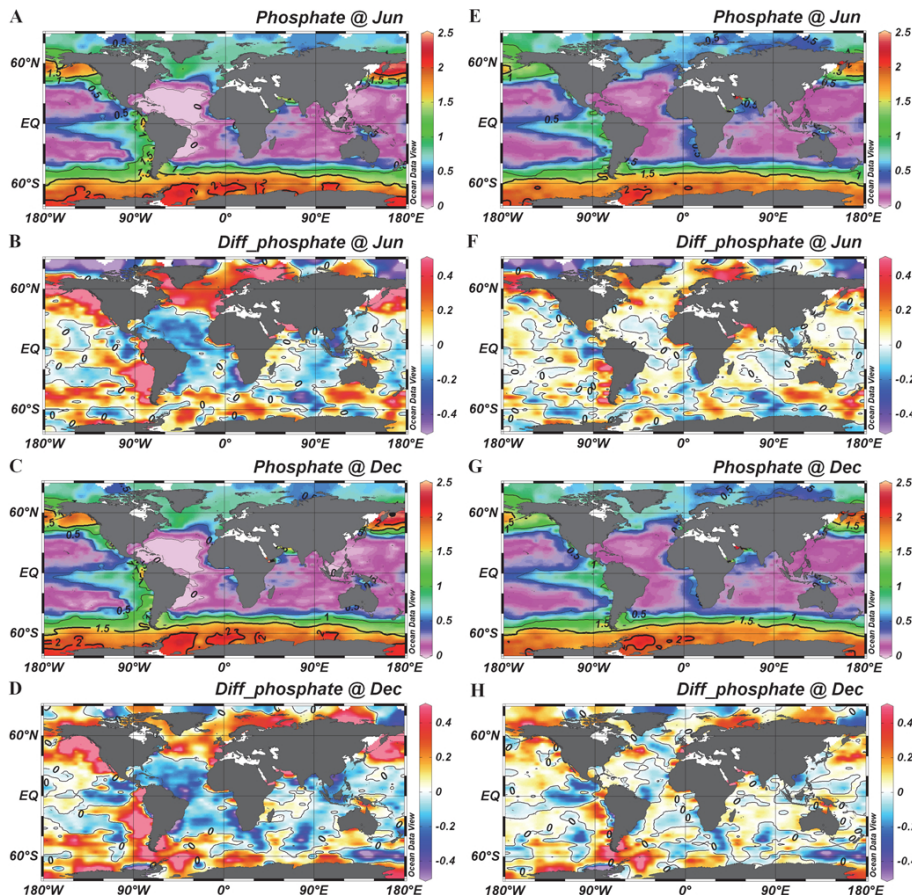


**Fig. 6.** Model-simulated phosphate (unit  $\mu\text{mol kg}^{-1}$ ) field of June and December, comparison of Exp A (A–D) and Exp B (E–H). Diff\_phosphate shows the difference between simulated and WOA phosphate, which is simulated phosphate minus WOA phosphate.

## Assimilating water column and satellite data

X. Yao and R. Schlitzer

Title Page

Abstract

Introduction

Conclusions

References

Tables

Figures

◀

▶

◀

▶

Back

Close

Full Screen / Esc

Printer-friendly Version

Interactive Discussion

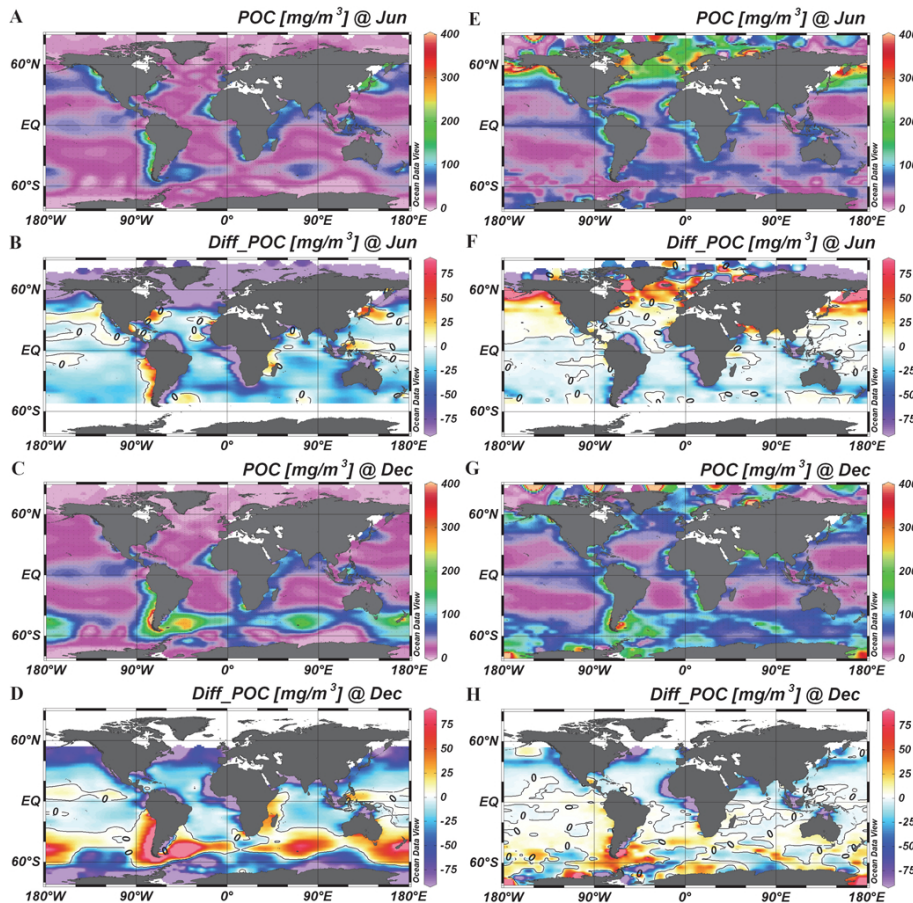


**Fig. 7.** Model-simulated POC field of June and December, comparison of Exp A (A–D) and Exp B (E–H). Diff\_POC shows the difference between simulated and satellite POC, which is simulated POC minus satellite POC.

## Assimilating water column and satellite data

X. Yao and R. Schlitzer

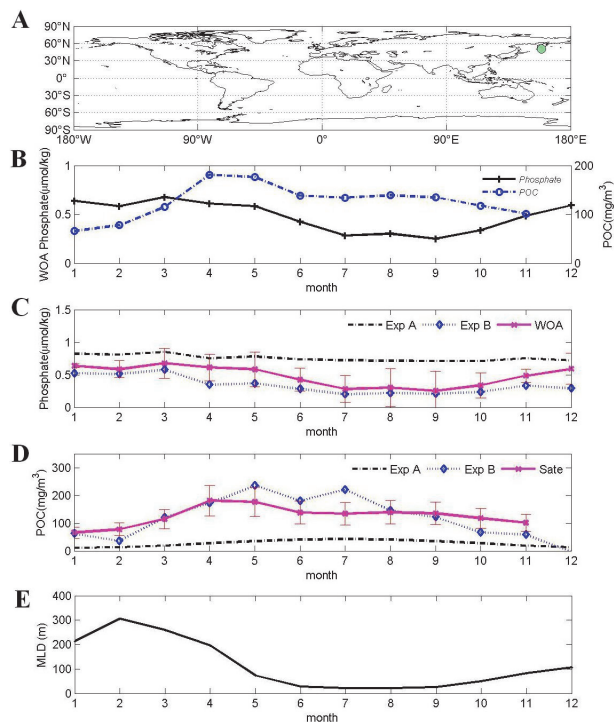


**Fig. 8.** Monthly phosphate and POC comparisons at the mid-latitude of the North Pacific Ocean. **(A)** position of this model point, **(B)** comparison of WOA phosphate and satellite POC, **(C)** comparison of model simulated phosphate of Exp A and Exp B with WOA phosphate, **(D)** comparison of model simulated POC of Exp A and Exp B with satellite POC. **(E)** Mixed Layer Depth (MLD) monthly evolution.

Title Page

Abstract

Introduction

Conclusions

References

Tables

Figures

◀

▶

◀

▶

Back

Close

Full Screen / Esc

Printer-friendly Version

Interactive Discussion



## Assimilating water column and satellite data

X. Yao and R. Schlitzer

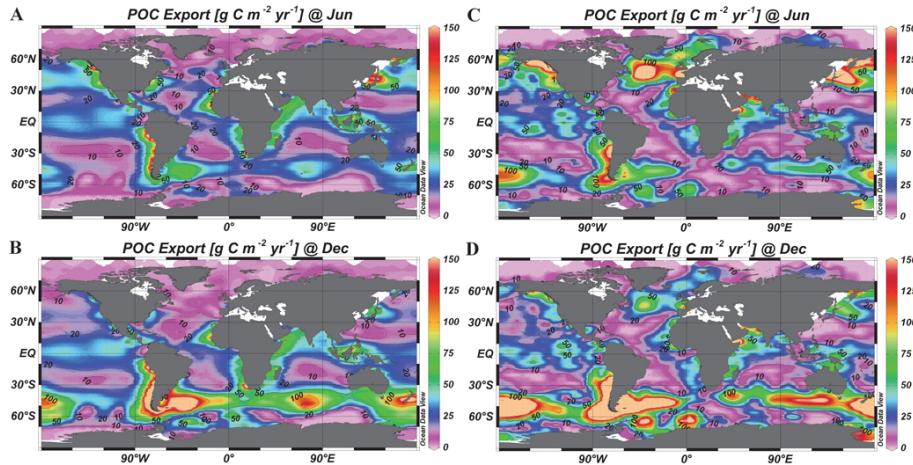


Fig. 9. Global POC export of Jun and Dec, Exp A (A, B) and Exp B (C, D).

Title Page

Abstract

Introduction

Conclusions

References

Tables

Figures

◀

▶

◀

▶

Back

Close

Full Screen / Esc

Printer-friendly Version

Interactive Discussion

